HHS Public Access

Author manuscript

Biomed Mater. Author manuscript; available in PMC 2017 November 04.

Published in final edited form as:

Biomed Mater. ; 11(6): 065008. doi:10.1088/1748-6041/11/6/065008.

Hydrogel fibers encapsulating hiPSC-MSCs, hESC-MSCs and hUCMSCs in injectable calcium phosphate scaffold for bone tissue engineering

Lin Wang[a,b], **Ping Wang**[b], **Michael D. Weir**[b], **Mark A. Reynolds**[b], **Liang Zhao**[*,b,c], and **Hockin H. K. Xu**[*,b,d,e]

[a] VIP Integrated Department, Stomatological Hospital of Jilin University, Changchun, Jilin 130011,China

[b] Department of Endodontics, Periodontics and Prosthodontics, University of Maryland School of Dentistry, Baltimore, MD 21201, USA

[c] Department of Orthopaedic Surgery, Nanfang Hospital, Southern Medical University, Guangzhou, Guangdong 510515, China

[d] Center for Stem Cell Biology & Regenerative Medicine, University of Maryland School of Medicine, Baltimore, MD 21201, USA

[e] Department of Mechanical Engineering, University of Maryland Baltimore County, Baltimore County, MD 21250, USA

Abstract

Human induced pluripotent stem cells (hiPSCs), human embryonic stem cells (hESCs) and human umbilical cord MSCs (hUCMSCs) are exciting cell sources for use in regenerative medicine. There has been no report on long hydrogel fibers encapsulating stem cells inside injectable calcium phosphate cement (CPC) scaffold for bone tissue engineering. The objectives of this study were to: (1) develop a novel injectable CPC construct containing hydrogel fibers encapsulating cells for bone engineering, and (2) investigate and compare cell viability, proliferation and osteogenic differentiation of hiPSC-MSCs, hESC-MSCs and hUCMSCs in injectable CPC. The stem cell-encapsulating pastes were fully injectable under a small injection force, and the injection did not harm the cells, compared to cells without injection ($p > 0.1$). Mechanical properties of stem cell-CPC construct were much higher than previous injectable polymers and hydrogels for cell delivery. hiPSC-MSCs, hESC-MSCs and hUCMSCs in hydrogel fibers in CPC had excellent proliferation and osteogenic differentiation. All three cells yielded high alkaline phosphatase, runt-related transcription factor, collagen I, and osteocalcin expressions (mean ± sd; $n = 6$). Cell-synthesized minerals increased substantially with time ($p < 0.05$), with no significant difference among the three types of cells ($p > 0.1$). Mineralization by hiPSC-MSCs, hESC-MSCs and hUCMSCs in CPC at 14 d was 13-fold that at 1 d. In conclusion, all three types of cells (hiPSC-

[*]**Correspondence:** Hockin H. K. Xu, Director, Biomaterials & Tissue Engineering Division, Department of Endodontics, Periodontics and Prosthodontics, University of Maryland School of Dentistry, Baltimore, MD 21201, hxu@umaryland.edu. Liang Zhao, Department of Orthopaedic Surgery, Southern Medical University, Guangzhou, Guangdong 510515, China, lzhaonf@126.com.

There is no conflict of interest.

MSCs, hESC-MSCs and hUCMSCs) in CPC scaffold showed high potential for bone tissue engineering, and the novel injectable CPC construct with cell-encapsulating hydrogel fibers is promising to enhance bone regeneration in dental, craniofacial and orthopedic applications.

Keywords

bone tissue engineering; calcium phosphate cement; human induced pluripotent stem cells; embryonic stem cells; umbilical cord stem cells; cell-encapsulating fibers

1. Introduction

Nearly seven million people suffer bone fractures in the United States, costing $2.5 billion annually [1]. This number is expected to increase as the life expectancy continues to rise. Bone tissue engineering involves the use of scaffolds, cells, and bioactive factors to facilitate the regeneration of bone defects arising from trauma, tumor, or bone-related diseases [2]. Stem cells are highly promising for tissue regeneration [3-7]. Human bone marrow mesenchymal stem cells (hBMSCs) have been extensively studied for tissue engineering [8]. However, autogenous hBMSCs require an invasive procedure to harvest, are limited in cell numbers, and have low self-renewal ability in seniors and patients with diseases [9]. Therefore, alternative stem cell sources are needed for bone regeneration.

Human umbilical cord MSCs (hUCMSCs) as a young and potent cell source, can be harvest without an invasion procedure, and are inexpensive and inexhaustible [10]. hUCMSCs can differentiate into multiple cell types, appear to cause no immunorejection, and are not tumorigenic in animal studies [11]. In addition, human embryonic stem cells (hESCs) are highly promising for regenerative medicine because of their rapid proliferation to provide an unlimited supply of stem cells. hESCs can differentiate into all bone-related cells, such as mesenchymal cells, osteoblasts, endothelial cells and neurons [12-14]. Indeed, progress has been achieved by seeding hESCs on scaffolds for tissue regeneration [15]. Recently, human induced pluripotent stem cells (hiPSCs) were generated from adult somatic cells by reprogramming techniques, and were presented as a promising source of progenitor cells [16]. Patient-specific hiPSCs can potentially differentiate into cells of all three germ layers [17]. hiPSCs are believed to be similar to hESCs in many aspects, including the expression of certain stem cell genes and proteins, doubling time, chromatin methylation patterns, embryoid body formation, viable chimera formation, potency, and differentiability [18]. MSCs were derived to reduce the risk of tumorigenesis of pluripotent stem cells and embryonic stem cells [19]. The resulting hiPSC-derived MSCs (hiPSC-MSCs) and hESC-derived MSCs (hESC-MSCs) are promising for regenerative therapy.

Scaffolds are needed in bone engineering. Pre-formed scaffolds have drawbacks including the difficulty in seeding cells deep into the scaffold, and inability for injection in minimally invasive surgeries [20]. Therefore, injectable hydrogel scaffolds have been developed [2]. However, injectable hydrogel scaffolds with cell encapsulation are not strong enough for loading-bearing uses [21]. They do not possess the mechanical strength to be used in load-bearing applications for bone regeneration [2]. To date, an injectable, bioactive, and mechanically-strong scaffold for stem cell encapsulation is unavailable for clinical use.

Previous studies encapsulated cells in alginate hydrogel microbeads, which were then mixed with a calcium phosphate cement (CPC) paste [22-24]. After injection, CPC sets to form a moderately load-bearing scaffold, and the microbeads degrade and release the cells throughout the CPC scaffold [22-24]. However, upon degradation, the microbeads create spherical pores in CPC with limited interconnection. Sufficient pore interconnection is required for cell migration, cell-cell interactions and tissue ingrowth. Fibers have advantage over beads because when fibers dissolve, then create long cylindrical channels throughout the CPC scaffold. Therefore, in the present study, stem cells were encapsulated in long alginate-fibrin hydrogel fibers which were then mixed into CPC for the first time.

The objectives of this study were to: (1) develop a novel injectable CPC construct containing hydrogel fibers encapsulating stem cells for bone engineering, and (2) investigate cell viability, proliferation and osteogenic differentiation by comparing hiPSC-MSCs, hESC-MSCs and hUCMSCs. The following hypotheses were tested: (1) CPC with stem cell-encapsulating fibers could be fully injectable, and the injection would not harm cells in the paste; (2) the injectable cell-encapsulating construct would have excellent mechanical properties; (3) hiPSC-MSCs, hESC-MSCs and hUCMSCs encapsulated in fibers in CPC would have excellent viability and proliferation, and can differentiate into osteogenic lineage; (4) all three types of cells in CPC would have high levels of osteogenic gene expressions, and synthesize bone minerals with similarly high potential for bone engineering.

2. Materials and methods

2.1. Culture of hiPSCs and derivation of MSCs

The use of hiPSCs, hESCs and hUCMSCs was approved by University of Maryland Institutional Review Board. The hiPSC BC1 line was derived from adult bone marrow CD34+ cells which were reprogramed by a single episomal vector pEB-C5, as previously described [25]. hiPSCs were maintained on mitotically-inactivated murine embryonic fibroblasts (MEF) feeder cells in hiPSC medium [25]. hiPSC medium consisted of 80% Dulbecco's modified Eagle medium (DMEM)/F12 (Invitrogen, Carlsbad, CA), 20% Knockout Serum Replacement (a serum-free formulation, Invitrogen), 1% MEM non-essential amino acids solution, 10 ng/mL basic fibroblast growth factor (β-FGF, Invitrogen), 1 mM L-glutamine (Sigma) and 0.1 mM β-mercaptoethanol (Sigma). hiPSCs were detached from a feeder layer and dissociated into clumps through treatment with 1 mg/mL collagenase type IV in DMEM/F12 at 37 °C for 6 min. The dissociated hiPSC clumps were collected by sedimentation, re-suspended in embryoid body (EB) differentiation medium (the same formulation as hiPSC culture medium but without β-FGF), and transferred to 25 cm^2 ultra-low attachment cell culture flasks (Corning, Corning, NY) [25].

After 10 d, the EBs were transferred onto 0.1% gelatin-coated culture dishes [25]. Cells growing out from EBs were cultured and upon 70% confluence, the outgrowth cells (P0) were selectively isolated by using cell scrapers and sub-cultured in MSC growth medium. This medium consisted of low glucose DMEM (Gibco, Grand Island, NY) supplemented with 10% fetal bovine serum (FBS, HyClone, Logan, UT), 100 U/mL penicillin and 100 mg/mL streptomycin (PS, Gibco). The differentiated cells from these culture conditions

were passaged until a homogeneous fibroblastic morphology appeared. They were termed hiPSC-derived MSCs (hiPSC-MSCs) [25]. Our previous study confirmed that the hiPSC-MSCs generated from this method expressed surface markers characteristic of MSCs (CD29, CD44, CD166, CD73), and were negative for typical hematopoietic (CD34), endothelial (CD31) and pluripotent markers (TRA-1-81 and OCT 3/4) [26]. The 4th passage hiPSC-MSCs were used in subsequent experiments.

2.2. Culture of hESCs and derivation of MSCs

The culture of hESCs (H9, Wicell, Madison, WI) followed the Wicell protocol. hESCs were first induced to form EBs following a protocol similar to that described for hiPSCs [5,27]. The out-growing cells were passaged until a homogeneous fibroblastic morphology appeared [5]. They were termed hESC-derived MSCs (hESC-MSCs) [5]. Our previous study confirmed that these hESC-MSCs express surface marker characteristic of MSCs (CD29, CD44, CD73 and CD166), and negative for hematopoietic markers (CD31, CD34, CD45) and pluripotent marker (TRA-1–81 and Oct3/4) [15]. The 4th passage hESC-MSCs were used.

2.3. hUCMSC culture

hUCMSCs were obtained from ScienCell (Carlsbad, CA), which were harvested from the Wharton's Jelly in umbilical cords of healthy babies. hUCMSCs were cultured in DMEM with 10% FBS and 1% PS [28]. Immunophenotyping via flow cytometry showed that hUCMSCs expressed high levels of adhesion markers (CD29 and CD44) and MSC-specific antigen CD105 (also call SH2), as described previously [28]. The cells were positive for HLA-class I (HLA-ABC), and negative for HLA-class II (HLA-DR). They did not express endothelial (CD31) or hematopoietic lineage markers (CD34 and CD45). This phenotype is characteristic for MSCs [28,29]. The 4th passage cells were used in subsequent experiments.

2.4. Cell encapsulation in alginate-fibrin fibers

Alginate was used for cell encapsulation because it is non-cytotoxic and can form ionic cross-link with multivalent cations under mild conditions without harming the cells [30]. However, alginate degrades slowly and uncontrollably. A previous study developed a method to control alginate gel degradation via partial periodate oxidation [31]. Our previous study used 7.5% oxidation and showed fast cell release from microbeads [23]. In the present study, alginate (64% guluronic acid, MW = 75,000-220,000 g/mol, ProNova, Oslo, Norway) was oxidized at 7.5% oxidation [23]. Cell-encapsulating alginate fibers were synthesized using a wet spinning technique, which consisted of the extrusion of a solution through a needle into a coagulation bath [32]. A 2% sodium alginate solution was prepared by dissolving alginate in a 155 mM sodium chloride solution at 37 °C. This was followed by adding fibrinogen from bovine plasma (Sigma) at a concentration of 0.4% [33]. Cells were added to the alginate-fibrinogen solution at a density of 1×10^6 cells/mL. The cell-alginate suspension was loaded into a 5 mL syringe. The cell-encapsulating alginate-fibrin fibers were obtained by extruding the cell-alginate suspension through a 27-gauge needle (with 210 μm inner diameter) via a syringe pump (NE-300 Single Syringe Pump, New Era Pump Systems, Farmingdale, NY) at a rate of 6 mL/min. The cell-alginate suspension was extruded into a 100 mL bath which consisted of 100 mmol/L calcium chloride (Sigma) and 1 NIH units per

mL of thrombin (Sigma). When the alginate-fibrinogen streamed into the bath, the presence of Ca^{2+} ions initiated the ionotropic gelation by counterbalancing the negative charges of alginate, while the reaction between fibrinogen and thrombin produced fibrin [23,32]. The alginate-fibrin fibers were allowed to cross-link in the bath for 20 min [32]. Then the alginate-fibrin fibers were collected and washed with phosphate buffered saline (PBS). This method resulted in the cell-encapsulating alginate-fibrin fibers. These fibers were examined via a light microscope (TE2000-S, Nikon, Melville, NY). The fiber formed in the cross-linking bath was a single continuous fiber. During handling and for the ease of mixing with CPC paste, the fibers were broken into a length of 15 mm, as described in the following section. These cell-encapsulating alginate-fibrin fibers were referred to as “CAF”.

2.5. Injectability testing of CPC pastes containing cell-encapsulating fibers

CPC powder consisted of tetracalcium phosphate [TTCP: $Ca_4(PO_4)_2O$] and dicalcium phosphate anhydrous (DCPA: $CaHPO_4$) [24]. TTCP [$Ca_4(PO_4)_2O$] was synthesized using DCPA ($CaHPO_4$) and calcium carbonate (both from J.T. Baker, Philipsburg, NJ) which were mixed and heated at 1500 °C for 6 hours (h) in a furnace (Model 51333, Lindberg, Watertown, WI). The heated mixture was quenched to room temperature, ground in a ball mill (Retsch PM4, Brinkman, NY) and sieved to obtain TTCP powder with a median particle size of 5 μm. The commercial DCPA powder was ground for 24 h in the ball mill in 95% ethanol and sieved to obtain a median particle size of approximately 1 μm. Then the TTCP and DCPA powders were mixed at 1:3 molar ratio in a micro-mill (Bel-Alert Products, Pequannock, NJ) to form the CPC powder. Chitosan could render the CPC paste fast-setting and mechanically strong [34]. Therefore, chitosan lactate (Vanson, Redmond, WA) was mixed with water at chitosan/(chitosan + water) mass fractions of 0%, 5%, 10% and 15%, respectively, to serve as four different CPC liquids. The CAF were cut into lengths of approximately 15 mm and mixed with CPC paste at a fiber volume fraction of 50%. The CAF were flexible and were randomly bent and oriented in the CPC paste. For mechanical reinforcement, an absorbable suture fiber (Vicryl, polyglactin 910, Ethicon, Somerville, NJ) was cut to 3 mm length and mixed in CPC paste at 10% by volume, which could provide several weeks of the needed early-strength to CPC scaffold [35]. The 10% suture fibers and 50% alginate volume fraction in CPC were based on previous studies [24,36]. Since the chitosan and suture fiber additions influenced the paste injectability, testing was done vs. chitosan (0%, 5%, 10% and 15%) and suture fiber content (0%, 10%). Therefore, eight CPC pastes were tested for injectability (Chitosan is referred to as CN, and suture fiber is referred to as SU):

(1) CPC paste using water as liquid, 0% chitosan (referred to as CPC control);

(2) CPC paste using water as liquid, 0% chitosan + 50% cell-encapsulating alginate-fibrin fibers (referred to as CPC-CAF);

(3) CPC + 5% chitosan liquid + 50% cell-encapsulating alginate-fibrin fibers (referred to as CPC-5CN-CAF);

(4) CPC + 5% chitosan liquid + 50% cell-encapsulating alginate-fibrin fibers + 10% suture fibers (CPC-5CN-CAF-SU);

(5) CPC + 10% chitosan liquid + 50% cell-encapsulating alginate-fibrin fibers (CPC-10CN-CAF);

(6) CPC + 10% chitosan liquid + 50% cell-encapsulating alginate-fibrin fibers + 10% suture fibers (CPC-10CN-CAF-SU);

(7) CPC + 15% chitosan liquid + 50% cell-encapsulating alginate-fibrin fibers (CPC-15CN-CAF);

(8) CPC + 15% chitosan liquid + 50% cell-encapsulating alginate-fibrin fibers + 10% suture fibers (CPC-15CN-CAF-SU).

To test injectability, a 10 mL syringe (Free-Flo, Kerr, Romulus, MI) was used with an opening tip of 2.7 mm which is similar to the inner diameter of a 10-gauge needle, as in a previous study [24]. The 10-gauge needle was similar to spinal needles used in augmentation of osteoporotic vertebrae and the management of vertebral compression fractures. Each CPC powder and liquid (2:1 mass ratio) were mixed using an automatic mixer (Maxi Mix, Thermolyne, Dubuque, IA) for 15 s. The paste was placed into the syringe which was pressed via a computer-controlled Universal Testing Machine (MTS, Eden Prairie, MN) at a crosshead speed of 15 mm/min [18]. The percentage of extruded paste was determined as the mass of the extruded paste divided by the original paste mass in the syringe. The injection force was recorded by the computer and the maximum force during injection was used as the injection force for the specific paste [24]. Six samples were tested for each group.

2.6. Mechanical testing of CPC scaffold containing cell-encapsulating fibers

CPC paste was placed into a mold of 3×4×25 mm and incubated in a humidor for 4 h at 37 °C. The set CPC specimens were demolded and immersed in culture medium at 37 °C for 1 d [35]. A three-point flexural test with a span of 20 mm was used to fracture the specimens on the Universal Testing Machine at a displacement rate of 1 mm/min. Flexural strength was calculated by: $S = 3F_{max}L/(2bh^2)$, where F_{max} is the maximum load on the load-displacement (F-d) curve, L is span, b is specimen width and h is thickness. Elastic modulus was calculated by: $E = (F/d)(L^3/[4bh^3])$, where load F divided by displacement d is the slope in the linear elastic region. Six specimens were tested for each group.

2.7. Viability of encapsulated hESC-MSCs, hiPSC-MSCs and hUCMSCs

hiPSC-MSCs, hESC-MSCs and hUCMSCs were each encapsulated in alginate-fibrin fibers. To evaluate if the CPC paste mixing and injection would harm the encapsulated cells, cell viability was examined without injection and after injection in CPC-15CN-CAF-SU paste. The paste was injected from a 10 mL syringe as described above. The CPC paste was removed and the CAF were collected immediately after injection. The CAF were then stained with a live/dead kit. The percentage of live cells and the live cell density were measured.

To evaluate the cell release behavior from CAF, 200 μL of CAF with each cell type was added to a well with 2 mL MSC growth medium. At predetermined time points (1, 4, 7 and 14 d), the CAF morphology and cells were examined via optical microscope (TE2000-S,

Nikon) following a previous study [23]. To further examine the cell release from CAF inside the CPC, the CAF were placed inside the CPC paste, using a method described previously [37]. First, 0.1 g of a CPC paste was placed to cover the bottom of a well (15 mm diameter) of a 24-well plate and the CPC paste surface was flattened. Then, 200 μL of CAF was placed on the CPC, and another 0.1 g of CPC paste was used to completely cover the CAF. The purpose of this setup was to provide a flat bottom of CPC surface, so that the cells released from the CAF could attach to CPC to enable live/dead staining and microscopic examination. Ideally, the CAF should be randomly mixed with CPC paste; however, subsequently breaking the CPC scaffold for analysis would create rough and tortuous surfaces unusable for microscopic examination. In the present study, the CAF were completely trapped inside the CPC, enabling the test of cell survival inside CPC, which would rely on the interconnected pores in CPC for fluids and nutrition. The construct was incubated at 37 °C for 30 min, then 2 mL of the osteogenic medium was added to each well to submerge the construct. At 1, 4, 7 or 14 d, the constructs were opened and the bottom CPC layer was used for analysis. The bottom CPC layer was immersed in a live/dead staining solution (Invitrogen, Carlsbad, CA). For each cell type and each time period, six wells were used for live/dead staining, and six wells were used for cell proliferation assay. The cells were examined via epifluorescence microscopy (Eclipse TE-2000S, Nikon). Three images were taken at random locations for each sample, with 6 samples yielding 18 images for each cell type at each time point. The percentage of live cells was: $P_{Live} = N_{Live}/(N_{Live} + N_{Dead})$, where N_{Live} and N_{Dead} are the number of live and dead cells, respectively. Live cell density was calculated as: $D_{Live} = N_{Live}/A$, where A is the area of the image where N_{Live} was measured [10].

A cell counting kit (CCK-8, Dojindo, Tokyo, Japan) was used to evaluate cell proliferation from 1 to 14 d in CPC-CAF constructs. CCK-8 is based on the WST-8 reaction that produces an orange formazan dye in an amount that is directly related with the number of viable cells [38]. After breaking the CPC cover, the bottom CPC layer was immersed in 2 mL of culture medium containing 10% CCK-8, and incubated in dark for 1.5 h. Then 100 μL of the medium was transferred to a new 96-well plate. The cell proliferative rate was determined via the absorbance at an optical density of 450 nm (OD_{450nm}) using a microplate reader (SpectraMax M5, Molecular Devices, Sunnyvale, CA), following a previous study [38]. WST-8 was reduced by dehydrogenase activities in cells to give a yellow-color formazan dye, which was soluble in culture medium. The amount of formazan dye from dehydrogenase in cells was directly proportional to the number of living cells [38]. In addition, to investigate cell-CPC scaffold interactions, CPC-15CN-CAF-SU samples with cells at 14 d were examined via scanning electron microscopy (SEM, FEI Quanta 200, Hillsboro, OR, USA). The samples were dehydrated, sputter-coated with gold and then viewed in SEM.

2.8. Differentiation of encapsulated hESC-MSCs, hiPSC-MSCs and hUCMSCs

The aforementioned CPC-15CN-CAF-SU constructs containing the three types of cells were cultured in osteogenic medium. At 1, 4, 7 and 14 d, the total RNA of the collected cells was extracted with TRIzol reagent and PureLink RNA Mini Kit (Life Technologies). Briefly, total RNA was extracted from homogenized constructs using 500 μL of TRIzol for each

well. PureLink RNA Mini Kit was used for total RNA isolation and purification, following the manufacturer's instructions. The concentration and purity of total RNA was assessed using NanoDrop 2000™ (Thermo Scientific, Waltham, MA, US). The absorbance ratio of A260/A280 was used as an indicator of protein contamination. A total amount of 1,000 ng of RNA was used to perform the reverse transcription into cDNA using a High-Capacity cDNA Reverse Transcription kit (Applied Biosystems) in a thermal cycler (GenAmp PCR 2720, Applied Biosystems). TaqMan gene expression kits (Applied Biosystems) were used to quantify the targeted genes on human alkaline phosphatase (ALP, Hs00758162_ml), Runt-related transcription factor (RUNX2, Hs00231692_ml), collagen type-I, alpha 1 (COL1A1, Hs00164004_m1), osteocalcin (OC, Hs00609452_g1) and glyceraldehyde 3-phosphate dehydrogenase (GAPDH, Hs99999905_m1; reference gene). Relative expression was evaluated using the $2^{-\Delta\Delta Ct}$ method and normalized by C_t of housekeeping gene GAPDH. C_t of hiPSC-MSCs, hESC-MSCs, and hUCMSCs in control medium at 1 day served as calibrator. The 14 d culture followed previous studies [10,24,37].

2.9. Mineral synthesis via encapsulated hiPSC-MSCs, hESC-MSCs and hUCMSCs

The aforementioned CPC-15CN-CAF-SU encapsulating the three types of cells were cultured in osteogenic medium. After 1, 7 and 14 d, two methods were used to investigate mineral synthesis by the encapsulated cells in v*itro*. First, xylenol orange was used which is a fluorescent probe, can chelate to calcium and stains mineral into a red color. It is not harmful to cells and the staining can be performed on live cells [39]. Because CPC could chelate with xylenol orange, the method was modified to avoid a strong background in images. 200 μL of CAF was placed on the polystyrene bottom of each well of 24-well plate, then 0.1 g of CPC paste was used to completely cover the CAF. At 1, 7, or 14 d, CPC was removed, the CAF were incubated overnight in 2 mL of osteogenic medium containing xylenol orange at a concentration of 100 μM. In this way, only the CAF were stained, without interference from CPC which was removed and not stained. Mineral nodules were observed via epifluorescence microscopy (Eclipse TE-2000S, Nikon). The mineral area percentage was calculated as $A_{Mineral}/A_{Total}$, where $A_{Mineral}$ is the area of mineralization (red fluorescence) in the image, and A_{Total} is the total area of the image [24].

Second, separate CPC-15CN-CAF-SU constructs were cultured and Alizarin red S (ARS) staining was performed. The CPC bottom layer with the released cell attachment were washed with PBS, fixed in 10% formaldehyde, and staining with 2% ARS (Millipore, Billerica, MA) for 5 min, which stained calcium-rich deposits made by the cells into a dark red color [36,37,40]. An osteogenesis assay kit (Millipore) was used to extract the stained minerals and measure the Alizarin red concentration, following the manufacturer's instructions [36,37,40]. The ARS standard curve was made with a known concentration of the dye. The CPC scaffold with the same composition as the cell construct, except without cells, was cultured in the same medium for the same time periods and used as control. At each time period of culture, the CPC control's ARS concentration was subtracted from the ARS concentration of the CPC-15CN-CAF-SU constructs containing cells, to yield the net mineral concentration synthesized by the cells, following previous studies [36,37,40].

2.10. Statistical analyses

Statistical analyses were performed via Statistical Package for Social Sciences (SPSS 16.0, Chicago, IL). Significance was assessed by using one- and two-way analyses of variance (ANOVA), Turkey's multiple comparison test and Student-Newman-Keuls test were used at p of 0.05. All data were expressed as the mean value ± one standard deviation (SD).

3. Results

The CAF fiber diameter (mean ± sd; $n = 50$) was measured to be (220 ± 28) μm. The injectability results of CPC containing these fibers are plotted in Fig. 1: (A) Percentage of paste extruded, and (B) injection force (mean ± sd; $n = 6$). In (A), nearly all the CPC paste in the syringe was smoothly extruded, and there was no significant difference between all the groups ($p > 0.1$). In (B), while all the injection forces were relatively small, the forces for the other groups were significantly higher compared to CPC control ($p < 0.05$). Adding chitosan and suture fibers increased the injection force ($p < 0.05$). The maximum injection force for group 7 was (43.1 ± 7.9) N, which was still relatively small and could be readily performed manually by surgeons. These results demonstrate that all these CPC pastes were injectable.

The mechanical properties of CPC are plotted in Fig. 2: (A) Typical load-displacement curves, (B) flexural strength, and (C) elastic modulus (mean ± sd; $n = 6$). In (A), load-displacement curves are shown for CPC-15CN-CAF and CPC-15CN-CAF-SU as examples. Other materials had similar fracture behavior except with smaller peak loads at failure. Adding chitosan and suture enhanced the strength ($p < 0.05$). CPC-15CN-CAF-SU had the highest strength of (8.5 ± 0.8) MPa, which was more than 3-fold that of CPC control ($p < 0.05$). The three bars on the right side indicate the strengths of cancellous bone and other injectable carriers for cell delivery reported in the literature. Elastic moduli of the modified CPCs were lower than CPC control because CPC was brittle and stiff, while chitosan and suture were flexible. These results demonstrate that CPC-15CN-CAF-SU had mechanical properties exceeding those of cancellous bone and previous injectable cell carriers.

Fig. 3 shows hiPSC-MSCs encapsulated in hydrogel fibers without CPC and without injection, and hiPSC-MSCs mixed in CPC paste and injected: (A-B) cell live/dead staining images, (C) percentage of live cells, and (D) live cell density (mean ± sd; $n = 6$). The images for the other two types of cells were similar. Live/dead staining images showed little difference, indicating that the CPC paste mixing and injection did not significantly harm the cells. In addition, there was no noticeable difference between the three types of cells. This was verified in the quantitative measurements in (C) and (D) ($p > 0.1$).

The release of encapsulated cells from CAF to CPC is shown in Fig. 4: (A-L) Live/dead staining images. At 1 d, the cells were inside the hydrogel fibers and there was no cell release from the fibers. At 4 d, CAF degradation was noticeable and there were some released cells around the fibers. At 7 d, the hydrogel fibers appeared to have disintegrated and the cells were released and proliferated rapidly. At 14 d, cell proliferation progressed and nearly formed a confluent layer covering CPC. Examining six samples per cell type per time period indicated no significant difference among the three cell types. There were numerous live cells and few dead cell. The CAF-released cell proliferation results on CPC

are plotted in Fig. 4: (M) Percentage of live cells, (N) live cell density, and (O) cell proliferation measured via CCK-8 (mean ± sd; $n = 6$). In (M), the percentages of live cells were above 90% and significantly increased from 1 d to 14 d ($p < 0.05$). In (N), due to cell proliferation, the live cell density on CPC increased by about 10-fold from 1 to 14 d. In (O), the three types of cells had similarly good proliferation on CPC, with approximately a 10-fold increase from 1 to 14 d. There was no significant difference among the three types of cells ($p > 0.1$).

SEM examination of cell-scaffold interactions and osteogenic differentiation results of cells in CPC-CAF are plotted in Fig. 5: (A) Representative SEM image, and (B-E) ALP, RUNX2, COL1 and OC gene expressions, respectively (mean ± SD; n = 6). In (A), the cell body is indicated by “Cell”, which infiltrated in a pore in CPC scaffold. The cells developed long cytoplasmic extensions (arrows) attaching to CPC scaffold, demonstrating that CPC was biocompatible and suitable for cell adhesion. In (B), for ALP, high peaks occurred at 14 d, which were about 30-fold that at 1 d. RUNX2, COL1 and OC expressions increased at 4 d, which further increased at 7 and 14 d, with the 7 and 14 d peaks being statistically similar ($p > 0.1$). The folds of increase reached 6, 14 and 8 for RUNX2, COL1 and OC, respectively. For all four osteogenic markers, there was no significant difference in peak expressions among the three types of cells ($p > 0.1$). These results demonstrate that cells in CPC-CAF differentiated into the osteogenic lineage, and the encapsulated hiPSC-MSCs, hESC-MSCs and hUCMSCs had similar osteogenic potential.

Mineral synthesis by cells in CPC-CAF is shown in Fig. 6 via two methods: (A-D) xylenol orange staining, and (E-H) ARS staining. (A-C) show representative images of xylenol orange staining for hiPSC-MSCs; images for the other two types of cells were similar. In (D), the mineral synthesis (mean ± sd; $n = 6$) increased by about 6-fold from 1 d to 14 d ($p < 0.05$). (E-G) show representative images of ARS staining of hESC-MSCs; images of the other two types of cells were similar. From 1 d to 14 d, the red staining of the synthesized bone mineral matrix covering the CPC bottom surface became a denser and darker red. In (H), the cell-synthesized mineral concentration was increased by about 13 folds from 1 to 14 d ($p < 0.05$). For both (D) and (H), at each time period, there was no significant difference between hiPSC-MSCs, hESC-MSCs and hUCMSCs ($p > 0.1$).

4. Discussion

The present study derived MSCs from hiPSCs and hESCs, and compared hiPSC-MSCs, hESC-MSCs and hUCMSCs encapsulated in hydrogel fibers in injectable CPC for the first time. The oxidized alginate-fibrin fibers were shown to be suitable for cell encapsulation, and for protecting the cells from the CPC paste mixing and injection processes. Cells in alginate-fibrin fibers could be quickly released to start their attachment and proliferation in CPC scaffold. The injectable CPC, reinforced by chitosan and degradable suture fibers, had good affinity for cell attachment and showed no negative effect on cell viability after injection, comparing to cells without injection. All three types of stem cells underwent osteogenic differentiation in CPC. Therefore, this study showed that hiPSC-MSCs, hESC-MSCs and hUCMSCs are all promising cell sources for bone regeneration, and the novel injectable CPC-CAF can be used to deliver stem cells for bone tissue engineering.

Hydroxyapatite (HA) and other CaP bioceramics are of importance for bone repair due to their excellent biocompatibility and bioactivity [41-44]. When implanted in an osseous site, bioactive materials provide an ideal environment for cellular reaction and colonization by osteoblasts. This leads to a tissue response termed osteoconduction in which bone grows on and bonds to the implant, promoting a functional interface [45]. Indeed, hMSCs showed excellent viability and differentiation on HA scaffolds [46]. However, sintered HA implants are generally not bioresorbable. In addition, pre-formed bioceramics require machining and may leave gaps when fitted into a bone cavity. This could lead to increases in bone loss, trauma, and surgical time [20]. In contrast, CPC can be injected with intimate adaptation to complex defects [47], can be easily shaped for esthetics in dental and maxillofacial repairs, and is osteoconductive and bioresorbable. The present study showed that with increasing chitosan concentration as well as suture fiber incorporation, the injection force of CPC was increased. However, the maximum injection force of 43 N was still small. An injection force of less than 100 N required to extrude a cement paste containing a polymer gel was regarded as being “injectable” [47]. The CPC-15CN-CAF-SU paste of the present study was fully extruded at a much smaller force and hence can be regarded as being injectable.

Besides injectability, the mechanical properties of the set scaffold after injection are also important. The traditional CPC was relatively brittle and weak, and hence its use was limited to the reconstruction of non-stress-bearing bone [48,49]. In the present study, the flexural strength was increased with increasing the concentration of chitosan and with the addition of absorbable suture fibers. A previous study reported a tensile strength of 3.5 MPa for cancellous bone [50]. Other studies reported that the strength was 0.7 MPa for injectable polymeric carriers for cell delivery [51], and 0.1 MPa for hydrogels [21]. The elastic modulus was 0.30 GPa for cancellous bone, 0.008 GPa for injectable polymeric carriers and 0.0001 GPa for hydrogels. These carriers are meritorious for tissue engineering in no-loading bearing locations. In contrast, the injectable CPC-15CN-CAF-SU of the present study was much stronger mechanically, with potential for a wide range of moderate load-bearing bone repairs.

Cell delivery methods are important for tissue engineering [52,53]. Traditionally, a cell suspension is placed onto the surface of a scaffold, with limitations including low seeding efficacy and minimal cell penetration into the scaffold [54]. For CPC, it is not feasible to directly mix the cells into the paste, because the mixing forces and the ionic exchanges during CPC setting would harm the cells. Our previous studies developed alginate microbeads to encapsulate cells which were then mixed into CPC paste [15,23,37]. During the CPC setting and injection process, the microbeads protected the cells. After CPC had set, the microbeads then dissolved and released the cells inside CPC scaffold. However, microbeads degradation created spherical pores in CPC with limited pore interconnectivity; for example, a microbead with a diameter of 200 μm would create a 200 μm pore in CPC. Encapsulating cells in hydrogel fibers could be advantageous over microbeads. These cell-encapsulating fibers can degrade and release the cells in CPC, and create long macropore channels. For example, a fiber of 200 μm diameter and 15 mm length would create a long macropore of 200 μm in diameter and 15 mm in length. This is beneficial in allowing oxygen and nutrients to reach the internal cells, and in providing more space for cells to communicate with each other in CPC. Furthermore, the CPC-CAF method overcame the

drawback of using hydrogel alone without CPC. The drawback of hydrogel includes the incapability to withstand pressure in load-bearing sites and to maintain the shape and contour integrity [55]. Due to the fast-degradable CAF, after CPC setting, the cell release started at 4 d, followed by cell spreading and proliferation. The fast release of cells was due to the oxidized alginate and the fibrin formation via the reaction between fibrinogen and thrombin [23]. In addition, other applications of long hydrogel fibers loaded with cells could include the formation and ingrowth of blood vessels in CPC scaffold in *vivo*, which require further study.

Three types of cells were investigated in the present study. Previous studies showed that hUCMSCs had excellent osteogenic effect when delivered via CPC scaffolds [24]. hESCs are also promising for bone regeneration due to its high proliferation. In addition, hiPSCs from adult somatic cells had several features similar to hESCs. In the present study, MSCs was derived from hiPSCs and hESCs, because MSCs can self-renew and differentiate into various tissues including bone [12]. A previous report showed that hiPSC-MSCs and hUCMSCs had similar proliferation when seeded on CPC scaffold [29]. Another study reported that hESCs and hiPSCs had similar characteristics and therapeutic effects for nerve regeneration [56]. These results are consistent with the present study showing that hiPSC-MSCs, hESC-MSCs and hUCMSCs had similarly good proliferation in CPC constructs.

The encapsulated hiPSC-MSCs, hESC-MSCs and hUCMSCs in CPC showed elevated levels of ALP, RUNX2, COL1A1 and OC gene expressions. The cell-synthesized bone matrix minerals increased with time. This indicates that the encapsulated cells in CPC were differentiated into the osteogenic lineage. RT-PCT showed that the ALP and OC peaked at 14 d. RUNX2 and COL1A1 generally peaked at 7 d, although the 7 and 14 d peaks were not significantly different. ALP is a well-defined marker for osteogenic differentiation that is expressed in the early stage of MSC osteogenesis, and its up-regulation is a prerequisite for mineralization and subsequent maturing of bone [57]. RUNX2 is essential for osteoblastic differentiation and acts as regulatory factors involved in osteogenic-related gene expression [58]. ECM-related cell structure collagen I is another marker for bone formation. Collagen I mediates cell adhesion and osteoblast phenotype formation, and provides a template for mineralization. In addition, OC is a bone-specific protein synthesized by osteoblasts that represents a good marker for osteogenic maturation. Our previous study showed that MSCs could have ALP peaks at 7 d by directly seeding the cells on CPC scaffold [29]. However, in the present study, the cells were encapsulated in hydrogel fibers, which delayed the cell release in CPC scaffold, thereby delaying its ALP expression peak to 14 d. Similarly, a previous study with hMSCs encapsulated in alginate microbeads also exhibited ALP peak at 14 d [15]. A previous study reported OC peaking at 8 d [57]. In the present study, although the OC expressions at 7 d were quite high, the peaks at 14 d were slightly higher than those at 7 d, indicating that the OC expression of these cells may continue to increase after 8 d.

Previous studies reported that RUNX2 was bound with OC promoter and was expressed in osteochondral progenitors and in early stages of osteogenic differentiation [59]. The present study showed that RUNX2 was up-regulated from 4 d and peaked at 7 d for all three types of stem cells, and stayed high at 14 d. Previous studies showed that hypoxia inhibited the osteogenesis in hMSCs through direct down-regulation of RUNX2 [60]. The up-regulation

of RUNX2 indicates that the encapsulated cells in CPC-CAF likely did not have hypoxia. This is likely because the macroporous CPC allowed oxygen and nutrients infiltration into the scaffold. Therefore, the high expressions of RUNX2 and other osteogenic genes verified that hiPSC-MSCs, hESC-MSCs and hUCMSCs had excellent osteogenic differentiation when encapsulated in CPC-15CN-CAF-SU construct.

The osteogenic differentiation of cells in CPC-15CN-CAF-SU was further verified via mineralization. There was a substantial increase in mineral over time for hiPSC-MSCs, hESC-MSCs and hUCMSCs. However, at 14 d, xylenol orange was 6-fold that at 1 d, while ARS was 13-fold that at 1 d. This discrepancy was likely because xylenol orange shows the two-dimensional surface staining, while ARS reflects the three-dimensional volume of minerals produced by the cells. With increasing time, the result from ARS was depended on not only the increasing staining area, but also the greater thickness of the bone matrix synthesized by the cells. In the present study, both methods showed that: (1) There was a monotonic and substantial increase in cell mineralization with time for cells inside CPC-15CN-CAF-SU; (2) all three types of cells, hiPSC-MSCs, hESC-MSCs and hUCMSCs, synthesized bone minerals in CPC-15CN-CAF-SU; (3) the three types of cells had no significant difference in mineral synthesis. Therefore, hiPSC-MSCs, hESC-MSCs and hUCMSCs are all promising cell sources for bone tissue engineering, and the injectable and moderately load-bearing CPC-15CN-CAF-SU is promising to deliver stem cells for bone regeneration. Further in vivo experiment should be performed using an animal model to demonstrate the possibility of future clinical applications and to determine the effects of key variables in the injectable CPC-CAF-stem cell construct on bone regeneration efficacy.

5. Conclusion

This study developed an injectable CPC-hydrogel fiber-stem cell construct for the first time and compared hiPSC-MSCs, hESC-MSCs and hUCMSCs for bone tissue engineering. The mechanical properties of the injectable construct matched/exceeded those of cancellous bone, and were much higher than previous injectable cell-encapsulating polymers and hydrogels. The injection did not harm the viability of the encapsulated cells. hiPSC-MSCs, hESC-MSCs and hUCMSCs in CPC-15CN-CAF-SU all had excellent proliferation and differentiated into the osteogenic lineage, with highly elevated ALP, RUNX2, COL1A1 and OC expressions. The mineralization of hiPSC-MSCs, hESC-MSCs and hUCMSCs in the injectable scaffold substantially increased over time. These results indicate that iPSC-MSCs, hESC-MSCs and hUCMSCs are all promising cell sources for bone engineering. The novel injectable CPC scaffold with cell-encapsulating hydrogel fibers is promising for stem cell delivery to enhance bone regeneration in dental, craniofacial and orthopedic applications.

Acknowledgements

We thank Prof. Linzhao Cheng of Johns Hopkins University for generously providing the hiPSC BC1 cells. This study was supported by NIH R01 DE14190 (HX) and R21 DE22625 (HX), National Science Foundation of China NSFC 81400487 (LW), Jilin Youth Fund of Science and Technology 20150520043JH (LW), China Scholarship Council (LW), NSFC 31328008 (LZ), NSF Guangdong 20130010014253 (LZ) and 2014A030313275 (LZ), Guangdong Science and Technology Project 2012B010200024 (LZ), and University of Maryland School of Dentistry Seed grant (HX).

Reference

1. Johnson PC, Mikos AG, Fisher JP, Jansen JA. Strategic directions in tissue engineering. Tissue Eng. 2007; 13:2827–37. [PubMed: 18052823]
2. Drury JL, Mooney DJ. Hydrogels for tissue engineering: scaffold design variables and applications. Biomaterials. 2003; 24:4337–51. [PubMed: 12922147]
3. Xin X, Hussain M, Mao JJ. Continuing differentiation of human mesenchymal stem cells and induced chondrogenic and osteogenic lineages in electrospun PLGA nanofiber scaffold. Biomaterials. 2007; 28:316–25. [PubMed: 17010425]
4. Park H, Temenoff JS, Tabata Y, Caplan AI, Mikos AG. Injectable biodegradable hydrogel composites for rabbit marrow mesenchymal stem cell and growth factor delivery for cartilage tissue engineering. Biomaterials. 2007; 28:3217–27. [PubMed: 17445882]
5. Hwang NS, Varghese S, Lee HJ, Zhang Z, Ye Z, Bae J, Cheng L, Elisseeff J. In vivo commitment and functional tissue regeneration using human embryonic stem cell-derived mesenchymal cells. Proc. Natl. Acad. Sci. 2008; 105:20641–6. [PubMed: 19095799]
6. van Manen EH, Zhang W, Walboomers XF, Vazquez B, Yang F, Ji W, Yu N, Spear DJ, Jansen JA, Yelick PC. The influence of electrospun fibre scaffold orientation and nano-hydroxyapatite content on the development of tooth bud stem cells in vitro. Odontology. 2014; 102:14–21. [PubMed: 23011475]
7. Kumar G, Tison CK, Chatterjee K, Pine PS, McDaniel JH, Salit ML, Young MF, Simon CG. The determination of stem cell fate by 3D scaffold structures through the control of cell shape. Biomaterials. 2011; 32:9188–96. [PubMed: 21890197]
8. Reilly GC, Radin S, Chen AT, Ducheyne P. Differential alkaline phosphatase responses of rat and human bone marrow derived mesenchymal stem cells to 45S5 bioactive glass. Biomaterials. 2007; 28:4091–7. [PubMed: 17586040]
9. Shah BS, Clark PA, Moioli EK, Stroscio MA, Mao JJ. Labeling of mesenchymal stem cells by bioconjugated quantum dots. Nano Lett. 2007; 7:3071–9. [PubMed: 17887799]
10. Zhao L, Weir MD, Xu HH. Human umbilical cord stem cell encapsulation in calcium phosphate scaffolds for bone engineering. Biomaterials. 2010; 31:3848–57. [PubMed: 20149437]
11. Can A, Karahuseyinoglu S. Concise Review: Human Umbilical Cord Stroma with Regard to the Source of Fetus-Derived Stem Cells. Stem Cells. 2007; 25:2886–95. [PubMed: 17690177]
12. Lee H, Shamy GA, Elkabetz Y, Schofield CM, Harrsion NL, Panagiotakos G, Socci ND, Tabar V, Studer L. Directed differentiation and transplantation of human embryonic stem cell - derived motoneurons. Stem Cells. 2007; 25:1931–9. [PubMed: 17478583]
13. Kuznetsov SA, Cherman N, Robey PG. In vivo bone formation by progeny of human embryonic stem cells. Stem Cells Dev. 2010; 20:269–87. [PubMed: 20590404]
14. de Peppo GM, Svensson S, Lenneras M, Synnergren J, Stenberg J, Strehl R, Hyllner J, Thomsen P, Karlsson C. Human embryonic mesodermal progenitors highly resemble human mesenchymal stem cells and display high potential for tissue engineering applications. Tissue Eng. Part A. 2010; 16:2161–82. [PubMed: 20136402]
15. Tang M, Chen W, Weir MD, Thein-Han W, Xu HH. Human embryonic stem cell encapsulation in alginate microbeads in macroporous calcium phosphate cement for bone tissue engineering. Acta Biomater. 2012; 8:3436–45. [PubMed: 22633970]
16. Takahashi K, Tanabe K, Ohnuki M, Narita M, Ichisaka T, Tomoda K, Yamanaka S. Induction of pluripotent stem cells from adult human fibroblasts by defined factors. Cell. 2007; 131:861–72. [PubMed: 18035408]
17. Haase A, Olmer R, Schwanke K, Wunderlich S, Merkert S, Hess C, Zweigerdt R, Gruh I, Meyer J, Wagner S. Generation of induced pluripotent stem cells from human cord blood. Cell Stem Cell. 2009; 5:434–41. [PubMed: 19796623]
18. Nakagawa M, Koyanagi M, Tanabe K, Takahashi K, Ichisaka T, Aoi T, Okita K, Mochiduki Y, Takizawa N, Yamanaka S. Generation of induced pluripotent stem cells without Myc from mouse and human fibroblasts. Nat. Biotechnol. 2008; 26:101–6. [PubMed: 18059259]
19. Knoepfler PS. Deconstructing stem cell tumorigenicity: a roadmap to safe regenerative medicine. Stem Cells. 2009; 27:1050–6. [PubMed: 19415771]

20. Moreau JL, Xu HH. Mesenchymal stem cell proliferation and differentiation on an injectable calcium phosphate–chitosan composite scaffold. Biomaterials. 2009; 30:2675–82. [PubMed: 19187958]
21. Drury JL, Dennis RG, Mooney DJ. The tensile properties of alginate hydrogels. Biomaterials. 2004; 25:3187–99. [PubMed: 14980414]
22. Qiao P, Wang J, Xie Q, Li F, Dong L, Xu T. Injectable calcium phosphate–alginate–chitosan microencapsulated MC3T3-E1 cell paste for bone tissue engineering in vivo. Mat. Sci. Eng. C-Mater. 2013; 33:4633–9.
23. Zhou H, Xu HH. The fast release of stem cells from alginate-fibrin microbeads in injectable scaffolds for bone tissue engineering. Biomaterials. 2011; 32:7503–13. [PubMed: 21757229]
24. Zhao L, Weir MD, Xu HH. An injectable calcium phosphate-alginate hydrogel-umbilical cord mesenchymal stem cell paste for bone tissue engineering. Biomaterials. 2010; 31:6502–10. [PubMed: 20570346]
25. Chou BK, Mali P, Huang X, Ye Z, Dowey SN, Resar L MS, Zou C, Zhang YA, Tong J, Cheng L. Efficient human iPS cell derivation by a non-integrating plasmid from blood cells with unique epigenetic and gene expression signatures. Cell Res. 2011; 21:518–29. [PubMed: 21243013]
26. Tang M, Chen W, Liu J, Weir MD, Chen L, Xu HH. Human induced pluripotent stem cell-derived mesenchymal stem cell seeding on calcium phosphate scaffold for bone regeneration. Tissue Eng. Part A. 2014; 20:1295–305. [PubMed: 24279868]
27. Arpornmaeklong P, Brown SE, Wang Z, Krebsbach PH. Phenotypic characterization, osteoblastic differentiation, and bone regeneration capacity of human embryonic stem cell-derived mesenchymal stem cells. Stem Cells Dev. 2009; 18:955–68. [PubMed: 19327009]
28. Thein-Han W, Xu HH. Collagen-calcium phosphate cement scaffolds seeded with umbilical cord stem cells for bone tissue engineering. Tissue Eng. Part A. 2011; 17:2943–54. [PubMed: 21851269]
29. Wang P, Liu X, Zhao L, Weir MD, Sun J, Chen W, Man Y, Xu HH. Bone tissue engineering via human induced pluripotent, umbilical cord and bone marrow mesenchymal stem cells in rat cranium. Acta Biomater. 2015; 18:236–48. [PubMed: 25712391]
30. Anseth KS, Bowman CN, Brannon-Peppas L. Mechanical properties of hydrogels and their experimental determination. Biomaterials. 1996; 17:1647–57. [PubMed: 8866026]
31. Bouhadir KH, Lee KY, Alsberg E, Damm KL, Anderson KW, Mooney DJ. Degradation of partially oxidized alginate and its potential application for tissue engineering. Biotechnol. Progr. 2001; 17:945–50.
32. Mihaila SM, Popa EG, Reis RL, Marques AP, Gomes ME. Fabrication of endothelial cell-laden carrageenan microfibers for microvascularized bone tissue engineering applications. Biomacromolecules. 2014; 15:2849–60. [PubMed: 24963559]
33. HoáLee K. Novel PDMS cylindrical channels that generate coaxial flow, and application to fabrication of microfibers and particles. Lab Chip. 2010; 10:1856–61. [PubMed: 20454720]
34. Costa-Pinto AR, Reis RL, Neves NM. Scaffolds based bone tissue engineering: the role of chitosan. Tissue Eng. Part B. 2011; 17:331–47.
35. Xu HH, Simon CG. Self-hardening calcium phosphate composite scaffold for bone tissue engineering. J. Orthop. Res. 2004; 22:535–43. [PubMed: 15099632]
36. Wang P, Song Y, Weir MD, Sun J, Zhao L, Simon CG, Xu HH. A self-setting iPSMSC-alginate-calcium phosphate paste for bone tissue engineering. Dent. Mater. 2016; 32:252–63. [PubMed: 26743965]
37. Chen W, Zhou H, Weir MD, Bao C, Xu HH. Umbilical cord stem cells released from alginate–fibrin microbeads inside macroporous and biofunctionalized calcium phosphate cement for bone regeneration. Acta Biomater. 2012; 8:2297–306. [PubMed: 22391411]
38. Shi Y, Niedzinski JR, Samaniego A, Bogdansky S, Atkinson BL. Adipose-derived stem cells combined with a demineralized cancellous bone substrate for bone regeneration. Tissue Eng. Part A. 2012; 18:1313–21. [PubMed: 22500696]
39. Wang YH, Liu Y, Maye P, Rowe DW. Examination of mineralized nodule formation in living osteoblastic cultures using fluorescent dyes. Biotechnol. Progr. 2006; 22:1697–701.

40. Chen W, Liu J, Manuchehrabadi N, Weir MD, Zhu Z, Xu HH. Umbilical cord and bone marrow mesenchymal stem cell seeding on macroporous calcium phosphate for bone regeneration in rat cranial defects. Biomaterials. 2013; 34:9917–25. [PubMed: 24054499]
41. Habraken W, Wolke J, Jansen JA. Ceramic composites as matrices and scaffolds for drug delivery in tissue engineering. Adv. Drug Deliver. Rev. 2007; 59:234–48.
42. Bohner M. Physical and chemical aspects of calcium phosphates used in spinal surgery. Eur. Spine J. 2001; 10:S114–21. [PubMed: 11716008]
43. Navarro M, Ginebra M, Planell J, Barrias C, Barbosa M. In vitro degradation behavior of a novel bioresorbable composite material based on PLA and a soluble CaP glass. Acta Biomater. 2005; 1:411–9. [PubMed: 16701822]
44. Rahaman MN, Day DE, Bal BS, Fu Q, Jung SB, Bonewald LF, Tomsia AP. Bioactive glass in tissue engineering. Acta Biomater. 2011; 7:2355–73. [PubMed: 21421084]
45. Ducheyne P, Mauck RL, Smith DH. Biomaterials in the repair of sports injuries. Nat. Mater. 2012; 11:652–654. [PubMed: 22825010]
46. Mao J, Giannobile W, Helms J, Hollister S, Krebsbach P, Longaker M, Shi S. Craniofacial tissue engineering by stem cells. J. Dent. Res. 2006; 85:966–79. [PubMed: 17062735]
47. Bohner M, Baroud G. Injectability of calcium phosphate pastes. Biomaterials. 2005; 26:1553–63. [PubMed: 15522757]
48. Carey LE, Xu HH, Simon CG, Takagi S, Chow LC. Premixed rapid-setting calcium phosphate composites for bone repair. Biomaterials. 2005; 26:5002–14. [PubMed: 15769536]
49. Barralet J, Gaunt T, Wright A, Gibson I, Knowles J. Effect of porosity reduction by compaction on compressive strength and microstructure of calcium phosphate cement. J. Biomed. Mater. 2002; 63:1–9.
50. Damien CJ, Parsons JR. Bone graft and bone graft substitutes: a review of current technology and applications. J. Appl. Biomater. 1991:187–208. [PubMed: 10149083]
51. Shi X, Sitharaman B, Pham QP, Liang F, Wu K, Billups WE, Wilson LJ, Mikos AG. Fabrication of porous ultra-short single-walled carbon nanotube nanocomposite scaffolds for bone tissue engineering. Biomaterials. 2007; 28:4078–90. [PubMed: 17576009]
52. Wang L, Shelton R, Cooper P, Lawson M, Triffitt J, Barralet J. Evaluation of sodium alginate for bone marrow cell tissue engineering. Biomaterials. 2003; 24:3475–81. [PubMed: 12809776]
53. Ginebra MP, Traykova T, Planell J. Calcium phosphate cements as bone drug delivery systems: a review. J. Control. Release. 2006; 113:102–10. [PubMed: 16740332]
54. Saiz E, Zimmermann EA, Lee JS, Wegst UG, Tomsia AP. Perspectives on the role of nanotechnology in bone tissue engineering. Dent. Mater. 2013; 29:103–15. [PubMed: 22901861]
55. Lee KY, Mooney DJ. Alginate: properties and biomedical applications. Prog. Polym. Sci. 2012; 37:106–26. [PubMed: 22125349]
56. Wang A, Tang Z, Park IH, Zhu Y, Patel S, Daley GQ, Li S. Induced pluripotent stem cells for neural tissue engineering. Biomaterials. 2011; 32:5023–32. [PubMed: 21514663]
57. Kim K, Dean D, Mikos AG, Fisher JP. Effect of initial cell seeding density on early osteogenic signal expression of rat bone marrow stromal cells cultured on cross-linked poly (propylene fumarate) disks. Biomacromolecules. 2009; 10:1810–7. [PubMed: 19469498]
58. Wang L, Li C, Chen Y, Dong S, Chen X, Zhou Y. Poly (lactic-co-glycolic) acid/nanohydroxyapatite scaffold containing chitosan microspheres with adrenomedullin delivery for modulation activity of osteoblasts and vascular endothelial cells. BioMed Res. Int. 2013; 2013:530712. [PubMed: 23841075]
59. Ducy P, Zhang R, Geoffroy V, Ridall AL, Karsenty G. Osf2/Cbfa1:a transcriptional activator of osteoblast differentiation. Cell. 1997; 89:747–54. [PubMed: 9182762]
60. Xu N, Liu H, Qu F, Fan J, Mao K, Yin Y, Liu J, Geng Z, Wang Y. Hypoxia inhibits the differentiation of mesenchymal stem cells into osteoblasts by activation of Notch signaling. Exp. Mol. Pathol. 2013; 94:33–9. [PubMed: 22964414]

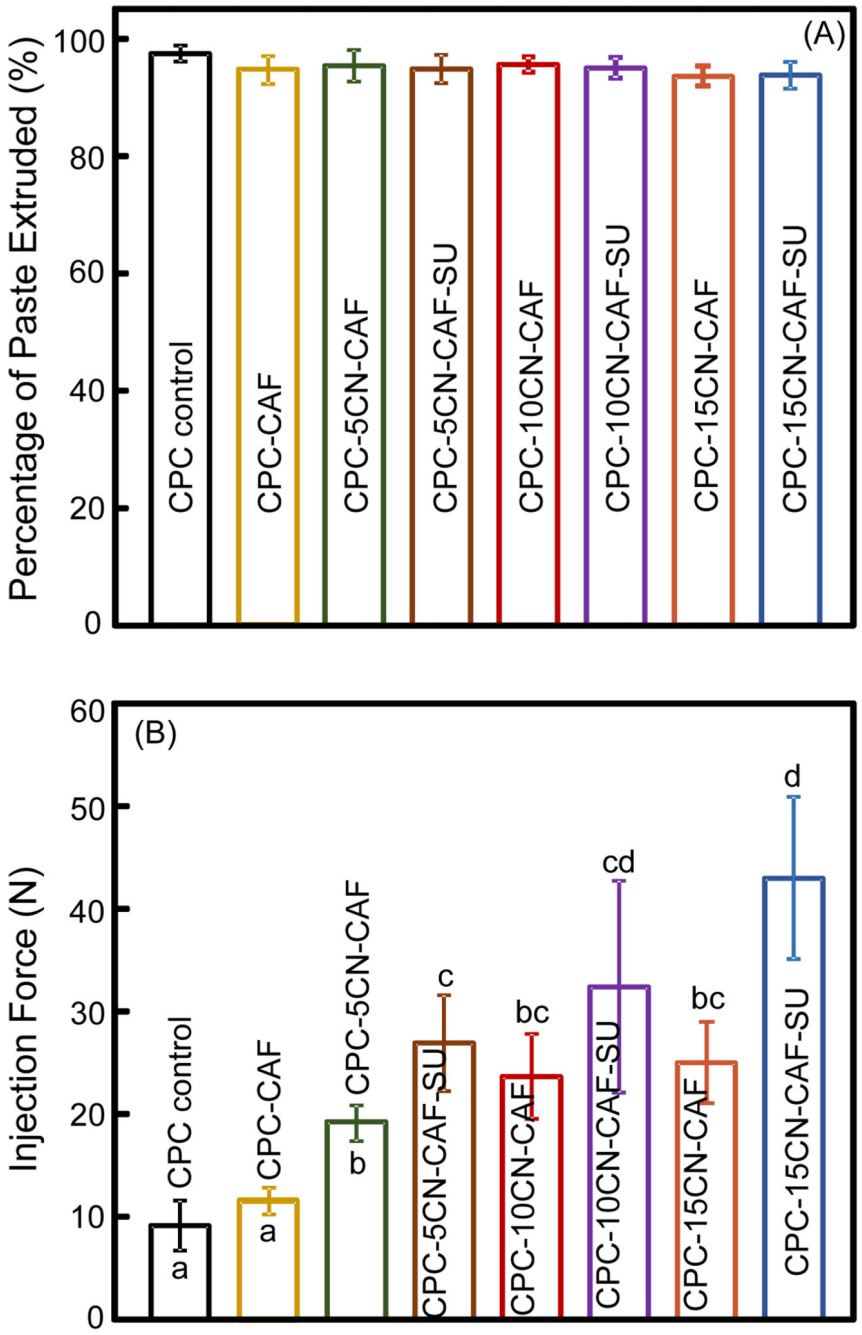

1.

Injectability of CPC-CAF pastes: (A) Percentage of paste extruded, and (B) injection force (mean ± sd; $n = 6$). CAF: cell-encapsulating alginate-fibrin fibers. CN: chitosan. SU: suture fibers. In (A), all values were not significantly different from each other ($p > 0.1$). In (B), bars indicated by different letters are significantly different ($p < 0.05$).

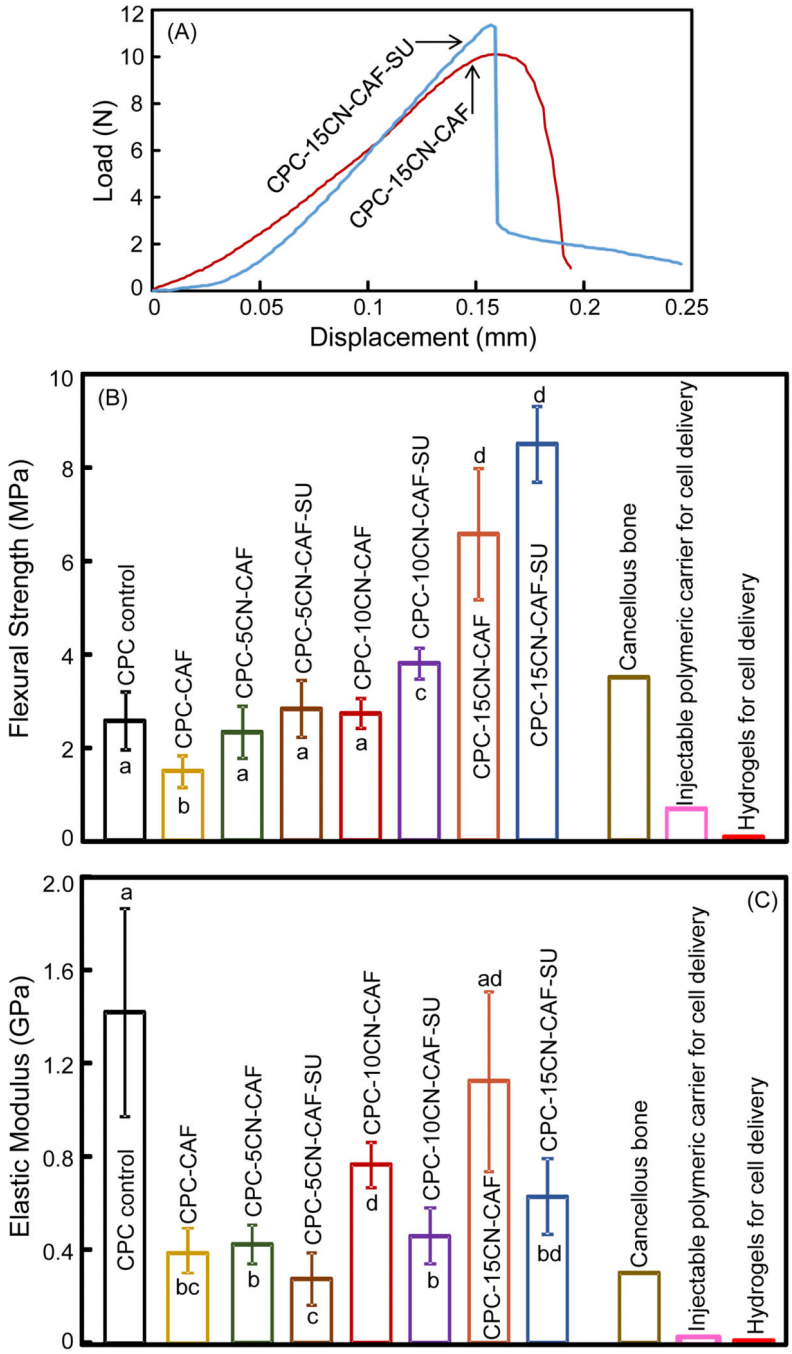

2.

Mechanical properties of CPC-CAF constructs: (A) Typical load-displacement curves, (B) flexural strength, and (B) elastic modulus (mean ± sd; $n = 6$). Load-displacement curves are shown for CPC-15CN-CAF and CPC-15CN-CAF-SU as examples. In (B and C), bars indicated by different letters are significantly different from each other ($p < 0.05$). Previously-reported values for cancellous bone, injectable cell-encapsulating polymer, and hydrogels are indicated by the three bars on the right side.

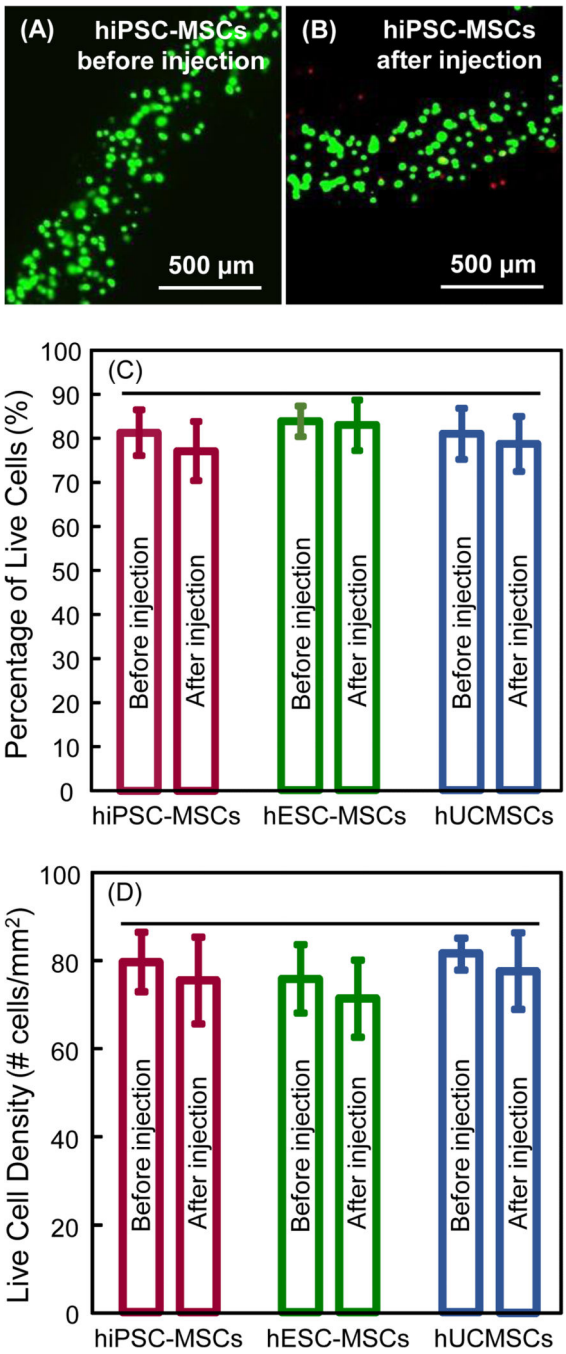

3.

Cell viability without injection and after injection: (A) hiPSC-MSCs in CAF (without CPC, without injection), and (B) hiPSC-MSCs in CAF after mixing with CPC paste and after injection. Live cells (green) were numerous. Dead cells (red) were few. (C): Percentage of live cells, and (D) live cell density (mean ± sd; $n = 6$). The CAF protected the cells, yielding viability after CPC mixing/injection to be similar to that without injection ($p > 0.1$). Horizontal line indicates values that are statistically similar ($p > 0.1$).

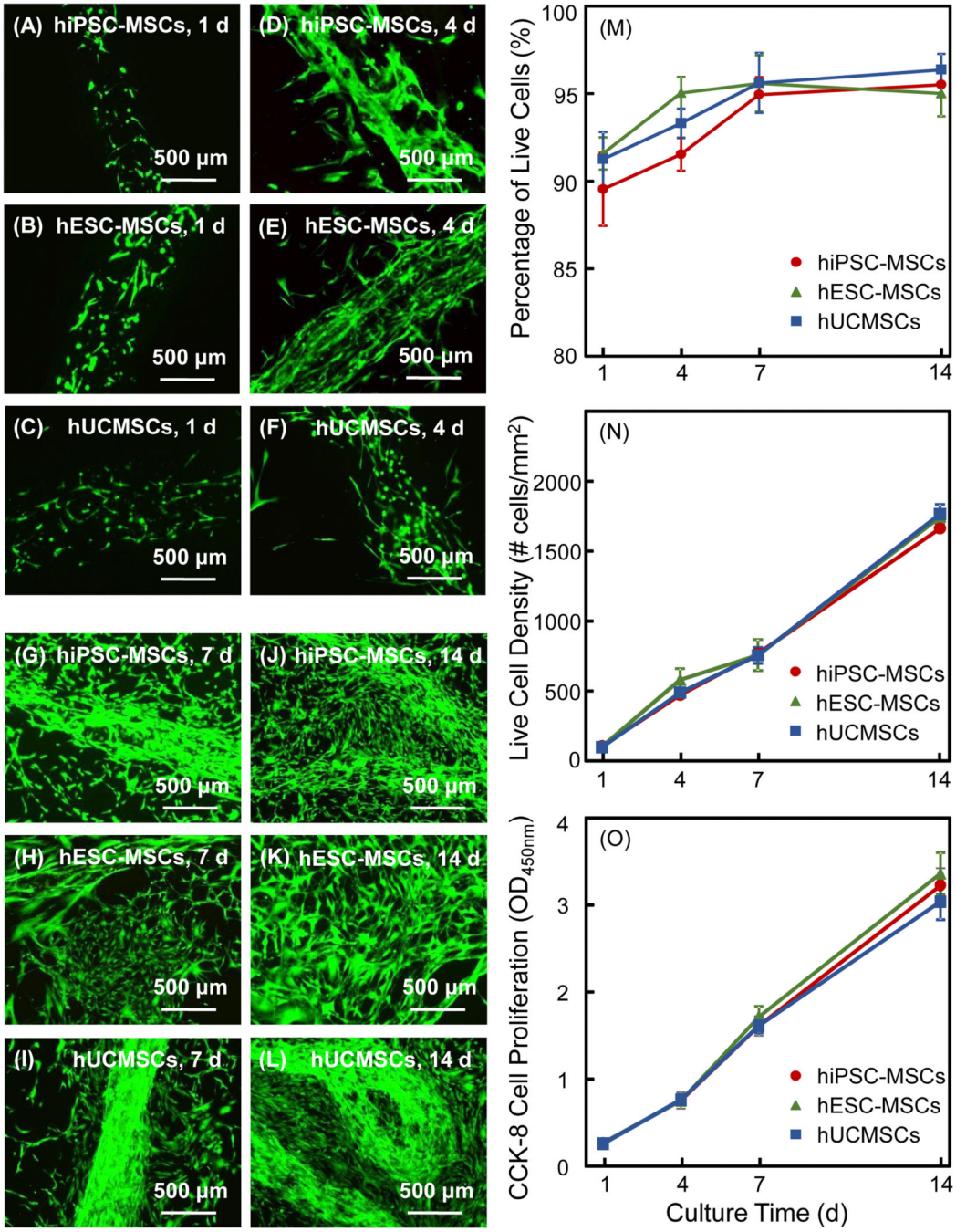

4.

Cell release from CAF and proliferation for hiPSC-MSCs, hESC-MSCs and hUCMSCs vs. time: (A-L) live/dead staining and fluorescence microscopy of cell release to CPC surface. In both cases, at 4 d, cells started to be released from fibers. From 7 to 14 d, more cells were released and the contours of fibers became obscure as they degraded. Live/dead images in showed numerous live cells with few dead cells, and the live cell numbers greatly increased from 1 to 14 d for all three cell types. Proliferation of hiPSC-MSCs, hESC-MSCs and

hUCMSCs in CPC-CAF constructs: (M) Percentage of live cells, (N) live cell density, and (O) CCK-8 cell proliferation (mean ± sd; $n = 6$).

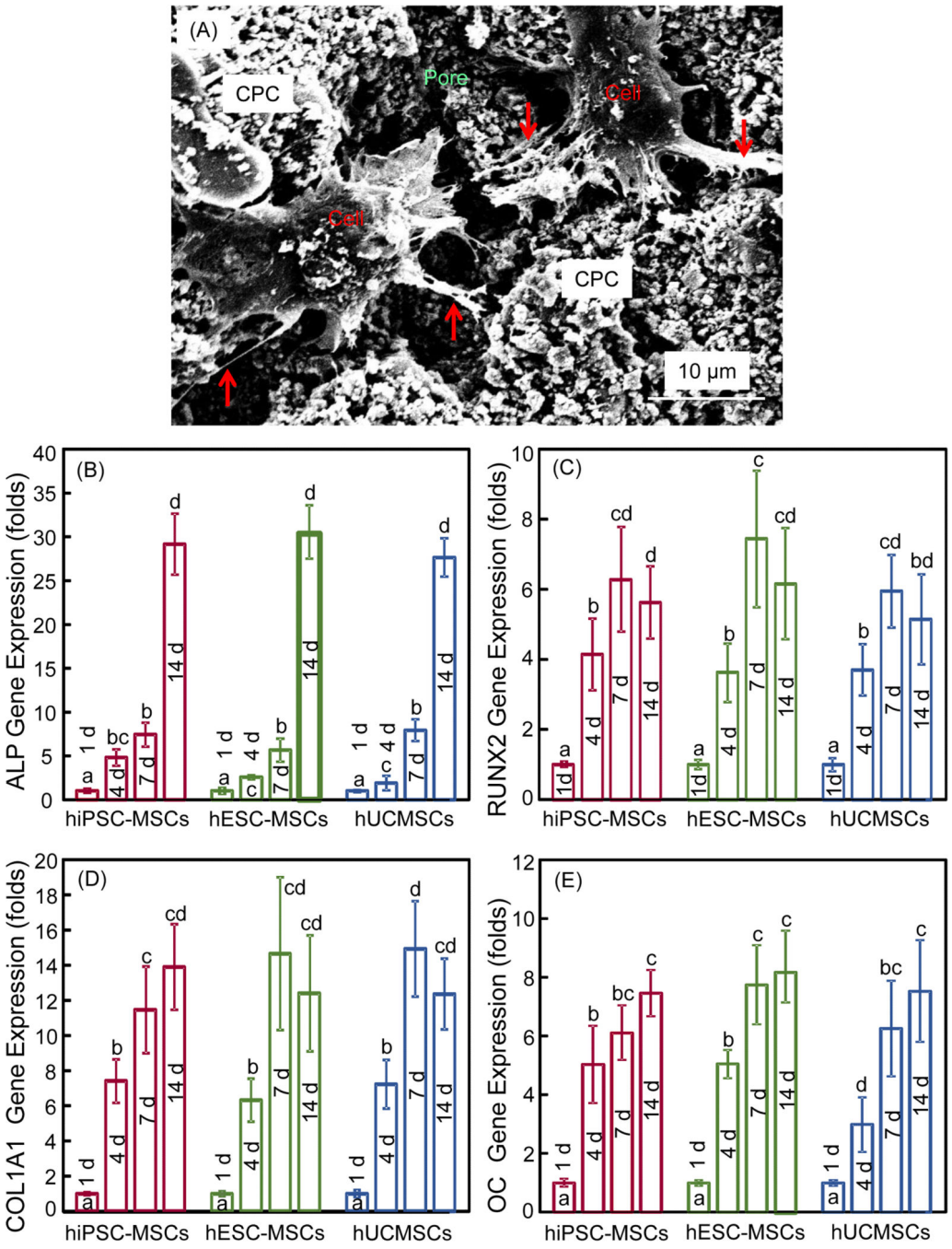

5.

SEM examination of cell-scaffold interactions and osteogenic differentiation of hiPSC-MSCs, hESC-MSCs and hUCMSCs in CPC-CAF constructs: (A) Typical SEM image of cells in a CPC pore (cytoplasmic extensions are indicated by arrows), (B) alkaline phosphatase activity (ALP), (B) runt-related transcription factor 2 (RUNX2), (C) collagen type I (COL1A1), (D) osteocalcin (OC) gene expressions (mean ± sd; $n = 6$). In each plot, values with dissimilar letters are significantly different ($p < 0.05$).

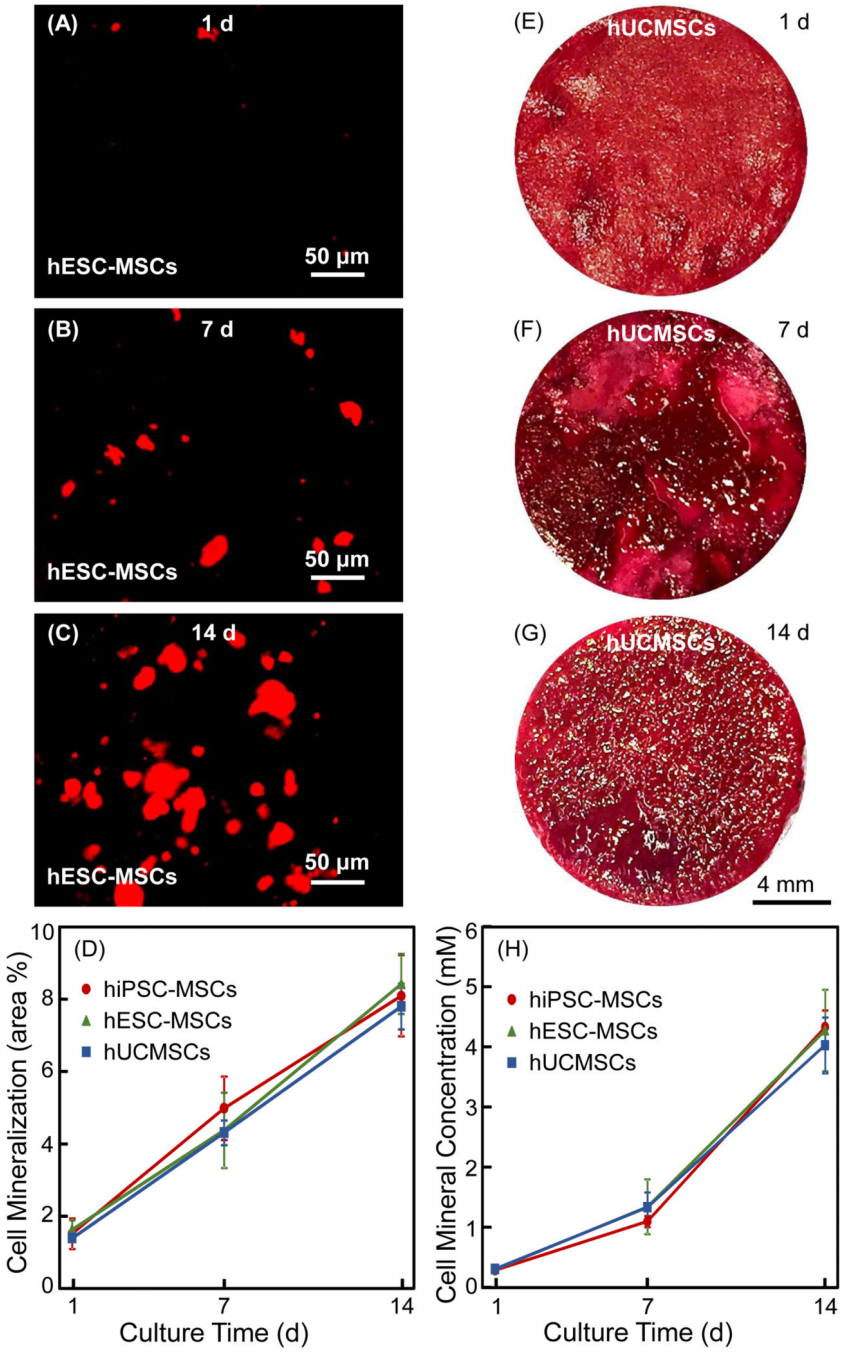

6.

Synthesis of bone minerals by encapsulated stem cells: (A-C) Xylenol orange mineral staining photos of hESC-MSCs (The other two cell types had similar images). (D) Xylenol orange mineral staining area fraction (mean ± sd; $n = 6$). (E-G) ARS staining images of hUCMSCs in CPC-CAF (The other two cell types had similar images). (H) ARS mineral concentration synthesized by cells in CPC-CAF measured by an osteogenesis assay (mean ± sd; $n = 6$).